


## FULL-LENGTH PAPER

# Structural dynamics of the complex of calmodulin with a minimal functional construct of eukaryotic elongation factor 2 kinase and the role of Thr348 autophosphorylation

Andrea Piserchio<sup>1</sup> | Kimberly Long<sup>2</sup> | Kwangwoon Lee<sup>1,3,8,9</sup> | Eric A. Kumar<sup>2</sup> | Rinat Abzalimov<sup>4</sup> | Kevin N. Dalby<sup>2,5</sup> | Ranajeet Ghose<sup>1,3,6,7</sup> 

<sup>1</sup>Department of Chemistry and Biochemistry, The City College of New York, New York, New York

<sup>2</sup>Division of Chemical Biology and Medicinal Chemistry, University of Texas, Austin, Texas

<sup>3</sup>Graduate Programs in Biochemistry, The Graduate Center of CUNY, New York, New York

<sup>4</sup>Biomolecular Mass Spectrometry Facility, CUNY ASRC, New York, New York

<sup>5</sup>Graduate Program in Cell and Molecular Biology, University of Texas, Austin, Texas

<sup>6</sup>Graduate Programs in Chemistry, The Graduate Center of CUNY, New York, New York

<sup>7</sup>Graduate Programs in Physics, The Graduate Center of CUNY, New York, New York

<sup>8</sup>Division of Genetics, Department of Medicine, Brigham and Women's Hospital, Harvard Medical School, Boston, Massachusetts

<sup>9</sup>Department of Biological Chemistry and Molecular Pharmacology, Harvard Medical School, Boston, Massachusetts

## Correspondence

Kevin N. Dalby, Division of Chemical Biology and Medicinal Chemistry, University of Texas, Austin, TX, USA.  
Email: dalby@austin.utexas.edu

Ranajeet Ghose, Department of Chemistry and Biochemistry, The City College of New York, New York, NY, USA.  
Email: rghose@ccny.cuny.edu

## Funding information

American Heart Association, Grant/Award Number: 15PRE25760018; National Institute of General Medical Sciences, Grant/Award Number: GM123252; Welch Foundation, Grant/Award Number: F-1390

## Abstract

The calmodulin (CaM) activated  $\alpha$ -kinase, eukaryotic elongation factor 2 kinase (eEF-2K), plays a central role in regulating translational elongation by phosphorylating eukaryotic elongation factor 2 (eEF-2), thereby reducing its ability to associate with the ribosome and suppressing global protein synthesis. Using TR (for truncated), a minimal functional construct of eEF-2K, and utilizing hydrogen/deuterium exchange mass spectrometry (HXMS), solution-state nuclear magnetic resonance (NMR) and biochemical approaches, we investigate the conformational changes accompanying complex formation between  $\text{Ca}^{2+}$ -CaM and TR and the effects of autophosphorylation of the latter at Thr348, its primary regulatory site. Our results suggest that a CaM C-lobe surface, complementary to the one involved in recognizing the calmodulin-binding domain (CBD) of TR, provides a secondary TR-interaction platform. CaM helix F, which is part of this secondary surface, responds to both Thr348 phosphorylation and pH changes, indicating its integration into an allosteric network that encompasses both components of the  $\text{Ca}^{2+}$ -CaM•TR complex. Solution NMR data suggest that  $\text{CaM}_{\text{H107K}}$ , which carries a helix F mutation, is

**Abbreviations:**  $\text{Ca}^{2+}$ -CaM,  $\text{Ca}^{2+}$ -loaded calmodulin; CaM, calmodulin;  $\text{CaM}_{\text{C}}$ , C-lobe of calmodulin;  $\text{CaM}_{\text{N}}$ , N-lobe of calmodulin; CBD, calmodulin-binding domain of eEF-2K; CTD, C-terminal domain of TR; eEF-2K, eukaryotic elongation factor 2 kinase; eEF-2, eukaryotic elongation factor 2; ESI-MS, electrospray ionization mass spectrometry; HMQC, heteronuclear multiple quantum correlation; HXMS, hydrogen/deuterium exchange mass spectrometry; KD, kinase domain of TR;  $\text{KD}_{\text{C}}$ , C-lobe of the kinase domain of TR;  $\text{KD}_{\text{N}}$ , N-lobe of the kinase domain of TR; NMR, nuclear magnetic resonance; PC, phosphorylated complex,  $\text{Ca}^{2+}$ -CaM•TR complex with TR phosphorylated on Thr348; pTR, TR phosphorylated on Thr348; R-loop, regulatory loop on eEF-2K; TR, truncated eEF-2K, a functional construct of eEF-2K; UC, unphosphorylated complex, same as the PC with unphosphorylated Thr348; XLMS, cross-linking mass spectrometry.

compromised in its ability to drive the conformational changes in TR necessary to enable efficient Thr348 phosphorylation. Biochemical studies confirm the diminished capacity of CaM<sub>H107K</sub> to induce TR autophosphorylation compared to wild-type CaM.

#### KEYWORDS

alpha kinase, calmodulin, hydrogen exchange mass spectrometry, solution NMR, translational elongation

## 1 | INTRODUCTION

Translation of an mRNA message into a polypeptide chain by the ribosome comprises of three broad stages: initiation, elongation and termination.<sup>1–4</sup> A critical step in elongation involves the translocation of the nascent polypeptide chain from the ribosomal A-site to the P-site to accommodate an incoming aminoacyl-tRNA. This process is driven by the activity of a ribosome-associated GTPase, eukaryotic elongation factor 2 (eEF-2).<sup>5–8</sup> Eukaryotic elongation factor 2 kinase (eEF-2K), a member of the  $\alpha$ -kinase family,<sup>9,10</sup> phosphorylates eEF-2,<sup>11–16</sup> reduces its affinity for the ribosome, and results in a reduction in global translational elongation rates.<sup>15,17,18</sup> eEF-2K is activated through a process dependent on calmodulin (CaM) (Figure S1A) but is distinct from the mechanisms deployed by other CaM-activated kinases.<sup>19</sup> A critical step in the activation of eEF-2K involves the autophosphorylation on Thr348 (three-letter codes used throughout for eEF-2K residues)<sup>20</sup> located at the N-terminal end of a regulatory loop (R-loop) following CaM-binding (Figure S1A). eEF-2K activity is modulated by a host of regulatory inputs that include Ca<sup>2+</sup> ions,<sup>21</sup> pH,<sup>22</sup> and additional phosphorylation events<sup>23</sup> occurring primarily on the R-loop. Given the critical role of eEF-2K in cellular physiology, its aberrant regulation has been implicated in various diseases that include several cancers<sup>24,25</sup> and neurological disorders.<sup>26,27</sup>

To aid in our long-term goal of obtaining a mechanistic understanding of the CaM-mediated activation of eEF-2K in atomic detail, we generated a minimal eEF-2K construct, TR (for truncated eEF-2K; Figure S1B), that is activated by Ca<sup>2+</sup>-CaM to a similar extent *in vitro* as the wild-type enzyme and retains its ability to efficiently phosphorylate eEF-2 in cells.<sup>28</sup> This construct, which contains Thr348 but is missing a significant section of the R-loop (and several phosphorylation sites therein), allows the generation of homogeneous samples monophosphorylated at position 348, making it ideal to specifically study the primary CaM-mediated activation process of eEF-2K driven by two key events (Figure S1A)—the

### Synopsis

Eukaryotic elongation factor 2 kinase (eEF-2K) regulates the elongation stage of protein synthesis by phosphorylating eukaryotic elongation factor 2 (eEF-2) and reducing its affinity for the ribosome. The activation of eEF-2K is mediated by calmodulin (CaM) and involves autophosphorylation at a primary regulatory site, Thr348. Utilizing TR, a minimal functional construct of eEF-2K, and various biophysical and complementary biochemical measurements, we analyze TR/CaM interactions and the effects of Thr348 phosphorylation thereon.

engagement of Ca<sup>2+</sup>-CaM and autophosphorylation on Thr348. Using hydrogen/deuterium exchange mass spectrometry (HXMS) and solution NMR studies, we had previously demonstrated large-scale changes in protection from solvent exchange for unphosphorylated TR upon forming a complex with Ca<sup>2+</sup>-CaM<sup>28</sup> (the unphosphorylated Ca<sup>2+</sup>-CaM•TR complex is referred to as the UC from hereon). Some of these changes were attributed to the extensive conformational reorganization within the kinase core that results in the almost 10,000-fold enhanced ability to autophosphorylate on Thr348 and generate the Ca<sup>2+</sup>-CaM•pTR complex (phosphorylated complex, PC from hereon)<sup>20</sup> *en route* to an active state that is capable of high efficiency substrate phosphorylation.

In the present study, we investigate the conformational changes of CaM upon transition from its free, Ca<sup>2+</sup>-saturated state to that bound to TR in the context of the UC (the Ca<sup>2+</sup>-CaM•TR complex), and then as part of the PC (the Ca<sup>2+</sup>-CaM•pTR complex) following Thr348 phosphorylation. Our results suggest an intimate interaction of the CaM C-lobe (CaM<sub>C</sub>) with TR that extends beyond its recognition of the CaM-binding domain (CBD) of the latter (Figure S1B). We further note that

CaM<sub>C</sub> acts as a sensor of remote events and responds to the phosphorylation of TR on Thr348. This contrasts the effects noted for TR itself upon Thr348 phosphorylation, where these changes are primarily restricted to regions that are spatially proximal to the phosphorylation site. A specific CaM<sub>C</sub> mutant (H107K), previously identified as compromised in its ability to activate eEF-2K,<sup>22</sup> cannot drive the extensive conformational changes that are a signature of the formation of the UC between wild-type CaM and TR.

## 2 | RESULTS

### 2.1 | The CaM C-lobe shows extensive protection upon binding TR

To complement our previous HXMS results<sup>28</sup> describing changes in the protection from <sup>2</sup>H exchange for TR upon the formation of the UC, we investigated the corresponding changes in Ca<sup>2+</sup>-CaM using HXMS data acquired at two different pH\* values (6.2 and 7.6; the “\*” indicates that the pH values were obtained through direct measurement) and four exchange times (1, 15, 30 and 60 min) to enable a robust statistical interpretation of the results. For CaM, 74 distinct peptides were identified, providing 94% coverage of its primary sequence to allow a detailed statistical analysis of <sup>2</sup>H incorporation therein. The degree of protection (expressed as a %; the superscript “b” indicates changes in protection induced by binding) was defined as

$$\mu_{CaM}^b = \Delta_{CaM,UC} - \Delta_{CaM,free} \quad (1)$$

where  $\Delta_{CaM,UC}$  and  $\Delta_{CaM,free}$  represent the percent <sup>2</sup>H incorporation in CaM as part of the UC and in the free, Ca<sup>2+</sup>-loaded state, respectively. Thus, values of  $\mu_{CaM}^b < 0$  indicate a lower level of <sup>2</sup>H incorporation in CaM when it is part of the UC compared to its free state, that is, increased protection upon complex formation. On average, as in the case of TR,<sup>28</sup> most of the identified CaM peptides experience an increase in protection upon UC formation. This change is more significant for CaM<sub>C</sub> compared to CaM<sub>N</sub> (Table S1).

To enable the structural interpretation of the changes in protection seen for Ca<sup>2+</sup>-CaM upon the formation of the UC, we projected the corresponding difference heatmaps (Figure S2) onto the structure of the complex of Ca<sup>2+</sup>-CaM with a peptide encompassing the isolated CBD (eEF-2K<sub>CBD</sub>).<sup>29</sup> The results for the 60 min time points, which are broadly representative of the overall trends, are shown in Figure 1 for each pH\* value. Data for CaM<sub>N</sub> suggest that regions in contact with the C-terminal tail of the

eEF-2K<sub>CBD</sub> (notably Pro98)<sup>29</sup> are better protected in the context of the UC, indicating that these same regions of CaM<sub>N</sub> contact TR, in agreement with our previous NMR studies.<sup>30</sup> Further, K30 (single-letter codes used for CaM residues) that has been shown to cross-link to Glu145 located on the N-lobe of the kinase domain of TR (KD<sub>N</sub>) within the UC in our cross-linking mass spectrometry (XLMS) studies,<sup>28</sup> is part of a group of residues that shows elevated levels of protection upon complex formation (Figure 1a). For CaM<sub>C</sub>, as expected, the hydrophobic pocket that comprises the primary binding site for eEF-2K<sub>CBD</sub> and hosts the 1-5-8 triad therein (Trp85-Ile89-Ala92)<sup>29</sup> experiences an increase in protection (Figure 1b). However, a widespread increase in protection is also detected on the surface opposite the one involved in recognizing the peptide, suggesting that this latter surface provides an additional interaction platform for TR within the UC. Our earlier NMR studies<sup>30</sup> had compared the chemical shifts of Ile- $\delta$ 1 and Met- $\epsilon$  methyl resonances of Ca<sup>2+</sup>-CaM in its complex with the isolated CBD with those of the corresponding residues in the UC. A relatively modest difference between the corresponding CaM<sub>C</sub> shifts ( $0.10 \pm 0.07$  ppm) was noted and attributed to some differences in domain orientation in the two complexes, a hypothesis supported by our previous XLMS measurements.<sup>28</sup> While differences in domain orientation are likely contributors, it is possible that the substantial chemical shift perturbations for M109 (helix F, 0.21 ppm), I125 (helix G, 0.12 ppm), and M145 (helix H, 0.13 ppm), at least in part, result from interactions involving this second CaM<sub>C</sub> surface with TR within the UC. These same NMR studies also suggest that the interaction of TR with CaM in the absence of Ca<sup>2+</sup> is driven almost entirely by CaM<sub>C</sub> (this interaction is mostly unmodified in the presence of Ca<sup>2+</sup> since CaM<sub>C</sub> remains Ca<sup>2+</sup>-free<sup>30</sup>). That such interactions occur with a significantly higher apparent affinity for TR ( $K_D \sim 77$  nM in the absence of Ca<sup>2+</sup>)<sup>30</sup> than with eEF-2K<sub>CBD</sub> ( $K_D \sim 35$   $\mu$ M in the absence of Ca<sup>2+</sup>)<sup>29</sup> suggests the presence of additional contacts that supplement the primary, CBD-driven interaction in the context of TR. Taken together, these data suggest an intimate association between CaM<sub>C</sub> and TR within the UC involving multiple regions/elements on the former.

In contrast to the increased protection mentioned above, consistent deprotection is seen for the first (AB-loop) and the C-terminal part of the third (EF-loop) Ca<sup>2+</sup>-binding loops located on CaM<sub>N</sub> and CaM<sub>C</sub>, respectively (Figure 1, Figure S2). Curiously, in contrast to the AB- and EF-loops, the CD-loop (CaM<sub>N</sub>) and the GH-loop (CaM<sub>C</sub>) show increased protection on average. This suggests that UC formation leads to a reorganization of the conformations of the Ca<sup>2+</sup>-binding loops in CaM. However, it is worth reiterating that the Ca<sup>2+</sup>-binding sites on

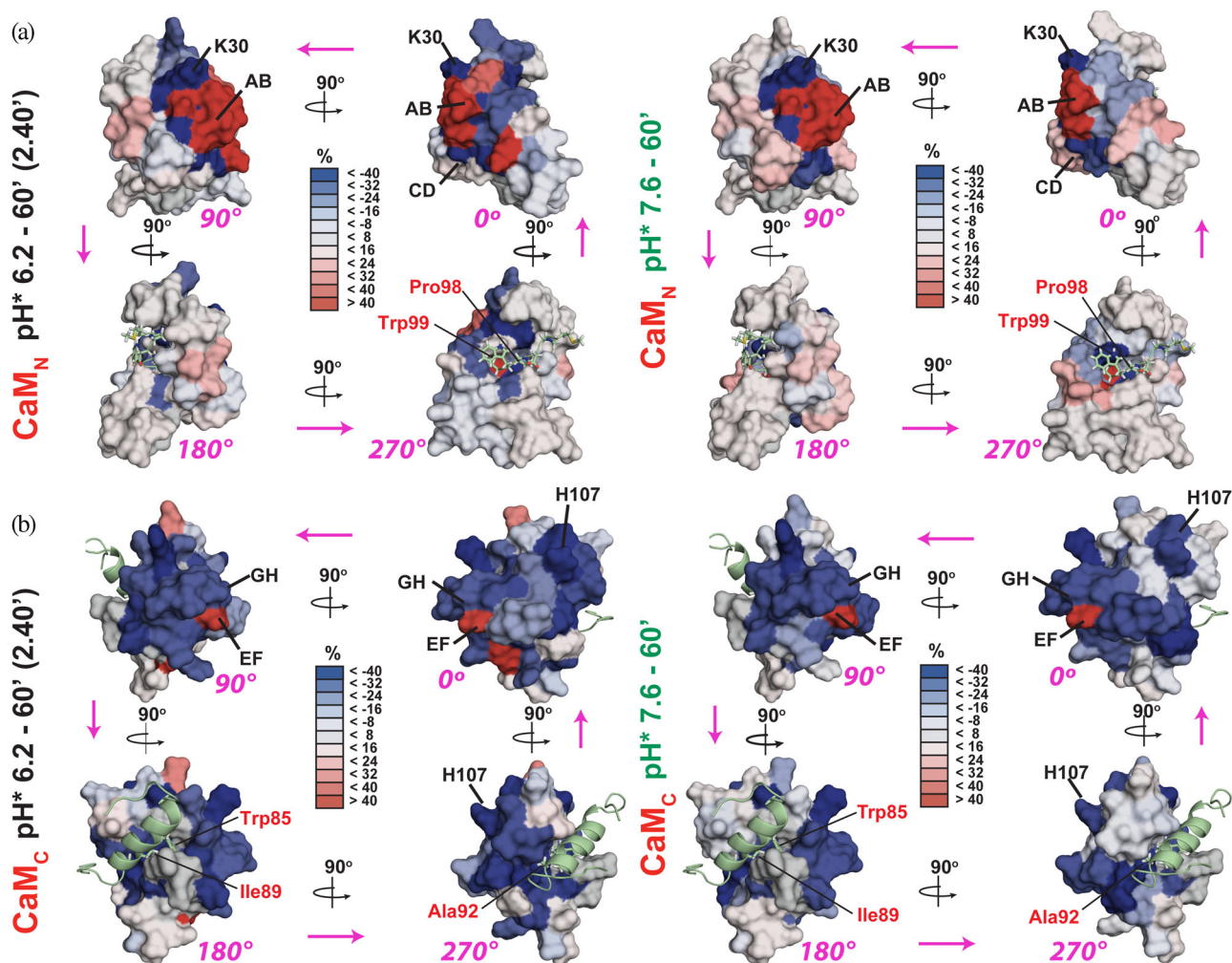


**FIGURE 1** Structural representation of the difference heatmaps for peptides derived from CaM comparing its free,  $\text{Ca}^{2+}$ -loaded state to that when it is part of the UC. Data for the 60 min timepoints for the experiments conducted at  $\text{pH}^* 6.2$  (left) and  $\text{pH}^* 7.6$  (right) are plotted on the molecular surfaces of (a)  $\text{CaM}_N$  and (b)  $\text{CaM}_C$ . The number in parenthesis (2.4 min) for the  $\text{pH}^* 6.2$  data represents the exchange time equivalent for the experiment conducted at  $\text{pH}^* 7.6$ . The lowest energy structure from the NMR ensemble of  $\text{Ca}^{2+}$ -CaM bound to the eEF-2K<sub>CBD</sub> peptide (PDB ID: 5J8H) is used. Locations of key structural elements of CaM discussed in the text are indicated and labeled in black. The bound eEF-2K<sub>CBD</sub> peptide is shown in ribbon representation with the sidechains of critical residues that participate in 1-5-8-(14) recognition of CaM are shown [Trp85-Ile89-Ala92-(Pro98)] and labeled in red (also indicated is Trp99). Data are plotted using a red-to-blue gradient, with red and blue representing decreased and increased protection, respectively, for CaM when incorporated into the UC compared to its free,  $\text{Ca}^{2+}$ -loaded state. The magenta arrows are provided to guide the eye to the anti-clockwise sequence of rotated structures in each case—starting with the top right panel ( $0^\circ$ ) to the top left panel ( $90^\circ$ ) to the bottom left panel ( $180^\circ$ ) to the bottom right panel ( $270^\circ$ ) and finally back to the top right panel

$\text{CaM}_C$  remain  $\text{Ca}^{2+}$ -free in the context of the UC.<sup>28</sup> The functional consequences of these changes, if any, are not immediately apparent.

## 2.2 | Effect of Thr348 phosphorylation

Next, we analyzed the changes in protection from solvent exchange in TR upon phosphorylation on Thr348 in the context of the UC, that is, upon transition from the UC to the PC. One hundred and twenty-three unique peptides

representing 83% of the primary sequence of TR were identified. The following quantity was defined (where the superscript “p” denotes changes in protection upon phosphorylation as opposed to binding as in Equation (1) above):

$$\mu_{TR}^p = \Delta_{TR,PC} - \Delta_{TR,UC} \quad (2)$$

$\Delta_{TR,PC}$ , and  $\Delta_{TR,UC}$  represent the percent  $^2\text{H}$  incorporation in TR as part of the PC and the UC, respectively. On average, a small increase in protection is seen, as

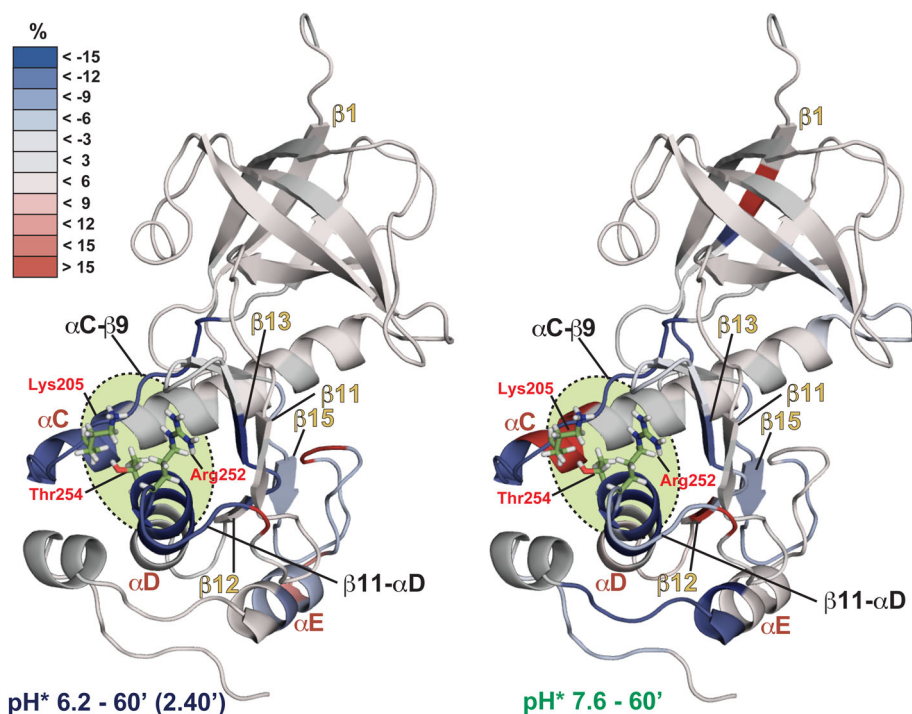
indicated by values of  $\mu_{TR}^p < 0$ , suggesting an overall rigidification of TR within its complex with CaM upon phosphorylation on Thr348. At the domain level, the kinase domain (KD), shows increased protection on average, while the C-terminal domain (CTD) remains largely unaffected (Table S2). At the local level, the difference heatmaps consistently localize the changes in protection for the KD to its C-lobe ( $KD_C$ ) (Figure S3). To enable the structural interpretation of these changes, we plotted the heat-maps corresponding to the 60 min timepoints on our molecular model of TR.<sup>28</sup> As shown for the KD in Figure 2, the most extensive changes in protection are seen on the C-terminus of  $\alpha C$ , the  $\alpha C$ - $\beta 9$  loop, the  $\beta 11$ - $\alpha D$  loop, and on helix  $\alpha D$ . These elements form part of the phosphate-binding pocket (PBP), housing the residues Lys205 ( $\alpha C$ - $\beta 9$ ), Arg252 ( $\beta 11$ - $\alpha D$ ) and Thr254 ( $\alpha D$ ) that are key in recognizing phosphorylated Thr348. The latter represents a critical step in the activation of eEF-2K<sup>20</sup> and constitutes a significant driver for efficient substrate phosphorylation (Figure S1A). Additional increases in protection are also noted for strand  $\beta 13$  that houses Asp274 and Gln276 that are involved in coordinating the phosphate groups of ATP and the  $-OH$  moiety of the substrate. Notably, changes in both  $k_{cat}$  and  $K_M$  have been deemed responsible for the almost 30-fold increase in specificity toward a peptide substrate observed upon autophosphorylation on Thr348.<sup>20</sup> While smaller than the ones noted for the KD, local changes in protection can be seen also in the CTD. Interestingly, the most significant of these are localized in the Gly569-Val585

segment (Figure S3) that is spatially proximal to the PBP in our structural model.<sup>28</sup> Taken together, these data imply that autophosphorylation on Thr348 and formation of the PC leads to conformational changes that, while mostly confined around the PBP in the  $KD_C$ , also extend to parts of the CTD.

We had previously utilized the  $\delta 1$ -positions of the 20 Ile residues on TR as probes of structure/dynamics changes upon binding CaM.<sup>28,30</sup> Using these same probes, we first assessed the effects of Thr348 phosphorylation on TR in the absence of CaM. A comparison of the  $^{13}C$ ,  $^1H$  HMQC spectra of unphosphorylated TR with that phosphorylated on Thr348 (Figure S4) suggests small but detectable perturbations in resonance positions. The most extensive changes are observed for the  $KD_C$  resonances corresponding to Ile271 and Ile275. Smaller changes are also detected for Ile209, Ile287, and, to some extent, for Ile214. Except for Ile214, all of these residues lie near the PBP, and these perturbations may be attributed to local changes in the environment originating from the engagement of the PBP by pThr38. The distal Ile107 on  $KD_N$  also shows a considerable reduction in intensity suggesting long-range communication even within the unbound, phosphorylated kinase.

Next, we compared the spectra of TR in the context of the UC with that in the context of the PC (Figure 3). As expected from the HXMS studies, the overall spectral perturbations remained subtle. However, they were enhanced in magnitude relative to the corresponding ones comparing TR and pTR in the

**FIGURE 2** Structural representation of the difference heatmaps for peptides derived from TR as part of the UC or the PC. Data for the 60 min timepoint for experiments conducted at pH\* 6.2 (left) and 7.6 (right) are plotted on the ribbon representation of our previously determined computational model of the TR KD.<sup>41</sup> Data are plotted using a red-to-blue gradient, red and blue representing decreased and increased protection for TR, respectively, as part of the PC compared to the UC. Key elements discussed in the text are labeled



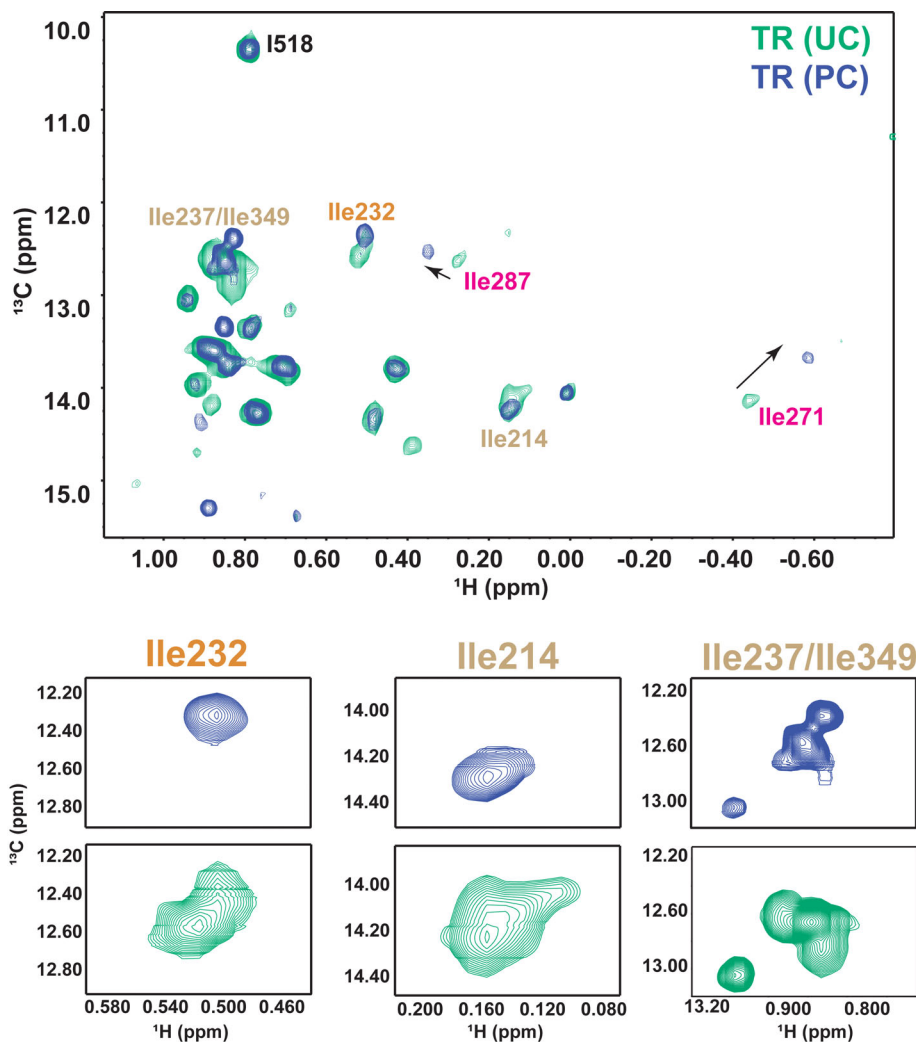


**FIGURE 3** Comparison between  $^{13}\text{C}$ ,  $^1\text{H}$  HMQC (700 MHz) spectra of I-labeled TR as part of the  $\text{Ca}^{2+}$ -CaM•TR (UC, green) or the  $\text{Ca}^{2+}$ -CaM•pTR (PC, blue) complexes. Key Ile- $\delta$ 1 resonances that show perturbations are indicated; chemical shift and lineshape changes are labeled in magenta and brown, respectively. Resonances that show both effects are labeled in orange. The bottom panels highlight the behaviors of selected resonances

absence of  $\text{Ca}^{2+}$ -CaM (compare Figures 3 and Figure S4). For the assigned peaks, enhanced chemical shift differences can be seen for Ile271 and Ile287, discussed above. In addition to chemical shift perturbations, the formation of the PC leads to the overall sharpening of the NMR resonances observed for Ile214 ( $\text{KD}_\text{N}$ ) and Ile232 (that lies on the loop that connects  $\text{KD}_\text{N}$  and  $\text{KD}_\text{C}$ ). Additional changes are seen for a cluster of resonances that includes Ile237 and Ile349 (Figure 3). While the Ile349 sidechain neighbors the phosphorylation site Thr348, all the other spectral changes suggest subtle conformational rearrangements in the kinase core. Overall, the NMR data largely reinforce the HXMS results showing that, while subtle changes occur at remote sites, the most substantial effects of Thr348 phosphorylation are felt in  $\text{KD}_\text{C}$ , most notably in and around the PBP.

Next, we measured the changes in  $^2\text{H}$  incorporation in CaM as part of the UC upon Thr348 phosphorylation and PC formation. These changes were quantified using

$$\mu_{\text{CaM}}^p = \Delta_{\text{CaM},\text{PC}} - \Delta_{\text{CaM},\text{UC}} \quad (3)$$

$\Delta_{\text{CaM},\text{PC}}$ , and  $\Delta_{\text{CaM},\text{UC}}$  represent the percent  $^2\text{H}$  incorporation in CaM as part of the PC and UC, respectively. While no significant changes are seen for  $\text{CaM}_\text{N}$ , a small but consistent increase in protection is seen in  $\text{CaM}_\text{C}$ , especially at the higher pH (Table S3). Analysis of local changes suggests that for  $\text{CaM}_\text{C}$ , most of helix F shows increased protection, that is,  $\mu_{\text{CaM}}^p < 0$  though significant deprotection ( $\mu_{\text{CaM}}^p > 0$ ) is seen in the adjoining EF-loop, with both effects being more pronounced at the higher pH (Figure S5). Representative changes at the 60 min timepoint mapped onto  $\text{CaM}_\text{C}$  in the structure of the  $\text{Ca}^{2+}$ -CaM•eEF-2K $_{\text{CBD}}$  complex are depicted in Figure 4. Note that the parts of  $\text{CaM}_\text{C}$  that respond to the phosphorylation of Thr348 on TR overlap with the secondary surface (opposite the one that accommodates the CBD) mentioned above. The fact that the CaM helix F experiences a significant increase in protection upon Thr348

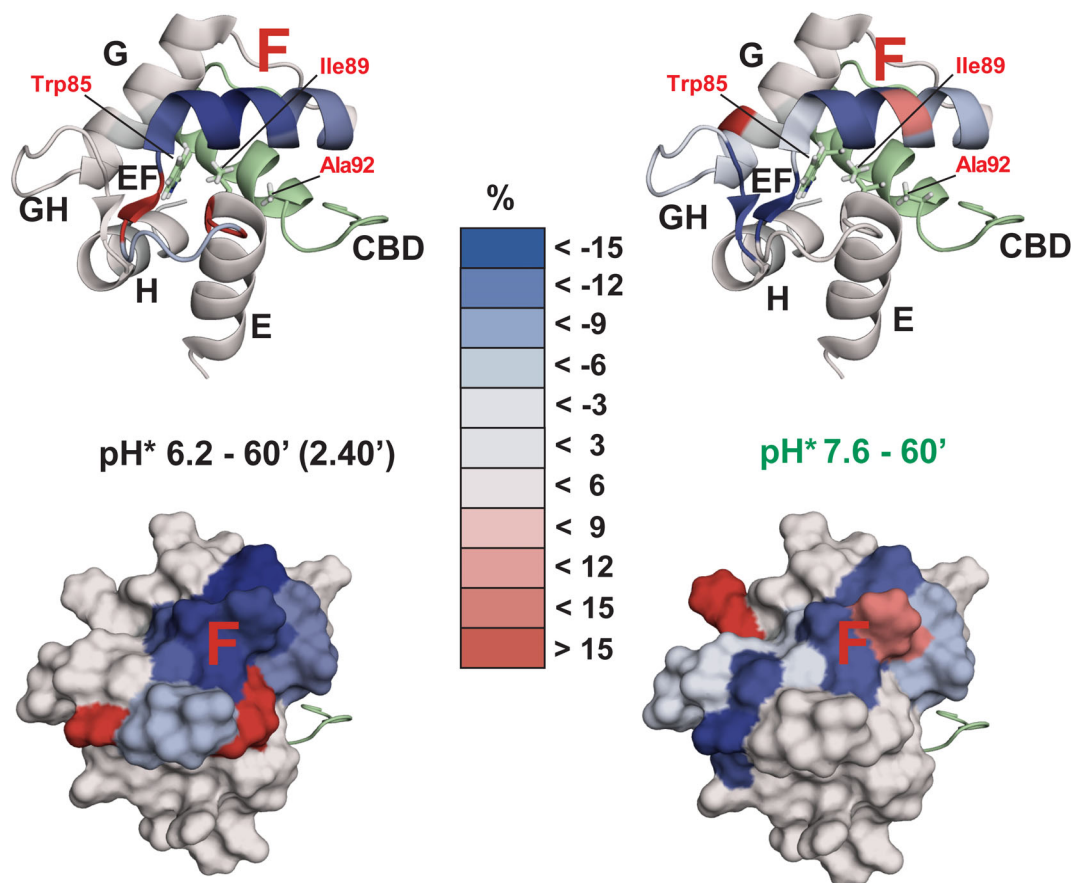


**FIGURE 4** Structural representation of the difference heatmaps for peptides originating from CaM<sub>C</sub> when part of the UC or the PC. Data for the 60 min timepoint at pH\* 6.2 (left) and 7.6 (right) are plotted using ribbon (top) or surface (bottom) representations of CaM<sub>C</sub> and the lowest energy structure from the NMR ensemble of Ca<sup>2+</sup>-CaM bound to the eEF-2K<sub>CBD</sub> peptide (PDB ID: 5J8H). Differences in protection are mapped using a blue (increased protection in the PC compared to the UC) to red (reduced protection in the PC) gradient. The helices and intervening loops are labeled; helix F that shows the most significant changes is indicated in large red font. The bound eEF-2K<sub>CBD</sub> peptide is shown as a ribbon and key residues therein (1-Trp85, 5-Ile89 and 8-Ala92) are indicated

phosphorylation provides additional support to a model in which this region of CaM directly interacts with TR and is intimately integrated with the overall allosteric signaling pathway.

### 2.3 | Effect of pH

It has been suggested that pH plays a significant role in the activity of eEF-2K, with a decrease in extracellular pH resulting in its activation.<sup>22</sup> Given that we acquired data at two distinct pH values, we explored if any pH-dependent changes in protection can be seen for the two constituents, CaM and TR/pTR, that form the UC/PC. Before quantitatively interpreting differences in solvent protection for data acquired at different pH values, the intrinsic pH dependence of amide exchange has to be accounted for. In the limit that the intrinsic opening ( $k_{op}$ ) and closing ( $k_{cl}$ ) rates are unaffected by the

pH, a change in the pH would, in effect, be equivalent to scaling the exchange time by a factor of  $10^{-\Delta\text{pH}}$ . In the present study, data collected at pH\* 6.2 using an exchange time  $t_1$  would then be identical to data acquired at pH\* 7.6 employing an exchange time of  $t_1 * 39.8 * 10^{-3}$ ; a 30 min dataset at pH\* 6.2 should be equivalent to a 1.2 min dataset at pH\* 7.6. Therefore, we reasoned that a direct comparison of the 30 min dataset at pH\* 6.2 with a 1.2 min dataset (we used the 1.0 min dataset as a reasonable approximation) at pH\* 7.6 should provide a measure of the structural and dynamic changes induced by pH.

Notably, free Ca<sup>2+</sup>-CaM is itself sensitive to changes in pH with respect to protection from solvent exchange. Lowering the pH leads to an overall increase in protection on CaM<sub>N</sub>. A more heterogeneous effect is seen for CaM<sub>C</sub>, where some increase in protection is seen towards the C-terminal end of the GH-loop and deprotection is seen on the F and G helices and towards the N-terminal end of the GH-loop. It is important to account for these

effects in determining the changes in the response of CaM to pH as part of the UC and the PC. Thus, the following quantities were defined:

$$\mu_{CaM,UC}^{pH} = \left[ \Delta_{CaM,UC} - \Delta_{CaM,free} \right]_{pH^*=6.2} - \left[ \Delta_{CaM,UC} - \Delta_{CaM,free} \right]_{pH^*=7.6} \quad (4a)$$

$$\mu_{CaM,PC}^{pH} = \left[ \Delta_{CaM,PC} - \Delta_{CaM,free} \right]_{pH^*=6.2} - \left[ \Delta_{CaM,PC} - \Delta_{CaM,free} \right]_{pH^*=7.6} \quad (4b)$$

Qualitatively similar patterns are seen for the  $\mu_{CaM,UC}^{pH}$  and the  $\mu_{CaM,PC}^{pH}$  values (Figure S6) suggesting a similar response to pH for CaM as part of either the UC or the PC. These data reflect that lowering the pH\* from 7.6 to 6.2 leads to a modest deprotection of CaM<sub>N</sub> and a more substantial increase in the protection of CaM<sub>C</sub>. For CaM<sub>C</sub>, the most significant increase in protection is seen for helix F in both the UC and PC, suggesting that elevated pH values may weaken the interactions of this secondary interface with CaM.

TR (and full-length wild-type eEF-2K) contains five His residues that have been suggested to contribute to its pH response.<sup>22</sup> These include three (His80, His87, and His94) on the CBD and two (His227 and His230) on the KD. No peptides corresponding to the CBD could be unambiguously identified in our current HXMS analyses. Hence, our studies do not provide any information on the former set. While the magnitudes of the pH-dependent changes in protection for TR (not shown), both as part of the UC and the PC, were similar to those for CaM, no significant changes were noted for  $\beta$ 10 that houses His227 and His230. Other changes were spatially diffuse and difficult to interpret in structural terms in the absence of additional information are not discussed further.

## 2.4 | A specific mutation on the CaM F-helix renders it incapable of driving substantial conformational transitions in TR

As noted above, in addition to the primary CaM<sub>C</sub> site that accommodates key hydrophobic residues of the TR CBD, there appears to be a secondary site on CaM<sub>C</sub> that reinforces the CaM/TR interaction. This predominantly hydrophilic surface encompasses helix F that, as described above, responds to both Thr348 phosphorylation and pH changes. It has been noted that a CaM variant carrying a specific mutation on this helix, CaM<sub>H107K</sub>, is compromised in its ability to activate eEF-2K.<sup>22</sup> We have previously shown<sup>28</sup> that interaction with Ca<sup>2+</sup>-CaM

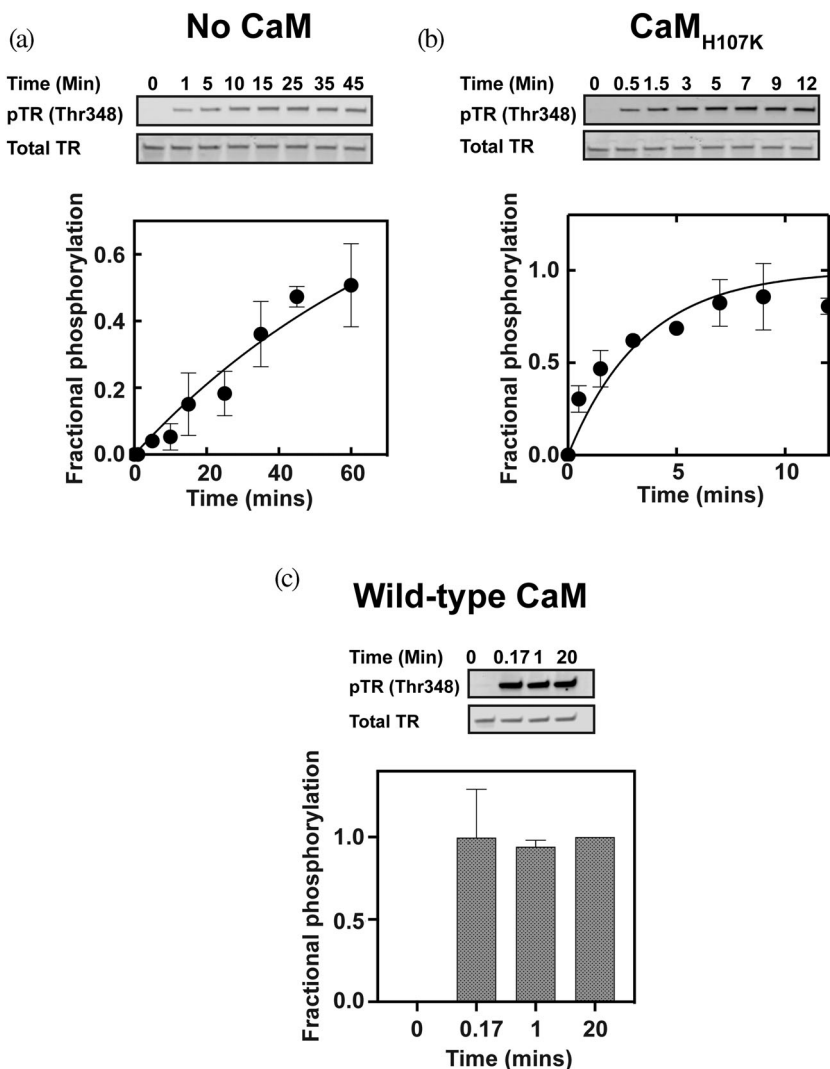
elicits significant perturbations in the Ile- $\delta$ 1 resonances of TR (Figure S7A). These perturbations likely reflect the Ca<sup>2+</sup>-CaM-induced conformational changes necessary to enable efficient phosphorylation on Thr348 (Figure S1A). The <sup>13</sup>C, <sup>1</sup>H HMQC spectrum of IM-labeled Ca<sup>2+</sup>-loaded CaM<sub>H107K</sub> is identical to the corresponding spectrum of wild-type CaM, indicating that this mutation does not lead to significant changes in the structure of CaM (Figure S7B). To test whether CaM<sub>H107K</sub> retains the ability to induce similar perturbations in TR as wild-type CaM, we monitored the changes in the Ile- $\delta$ 1 resonances of TR upon formation of a UC involving CaM<sub>H107K</sub>. The interaction of CaM<sub>H107K</sub> and unphosphorylated TR does not result in the widespread spectral changes in the TR spectrum as those induced by wild-type CaM (compare Figures S7A and S7C). Only minor changes are observed for one of the resonances of the Ile131/Ile215 cluster on KD<sub>N</sub>, and for Ile232 in the ATP binding loop. Other minor spectral variations include attenuation of the intensities for Ile209 in the inter-lobe linker, and Ile275 in the catalytic loop. Thus, these data suggest that CaM<sub>H107K</sub> is severely impaired in its ability to drive the conformational changes in TR that enable efficient phosphorylation on Thr348. Indeed, the intrinsic Thr348 autophosphorylation rate ( $t_{1/2} \sim 59$  min) is greatly enhanced by wild-type Ca<sup>2+</sup>-CaM, with the reaction being completed within 10 s ( $t_{1/2} < 0.17$  min; Figure 5). In contrast, while Ca<sup>2+</sup>-CaM<sub>H107K</sub> can drive Thr348 phosphorylation, it does so with a significantly reduced efficiency ( $t_{1/2} \sim 2.4$  min; Figure 5). Some of the small perturbations induced by CaM<sub>H107K</sub> on the spectrum of TR may reflect the generation of a conformation that is still capable of driving Thr348 autophosphorylation to some extent. It is interesting to note that some of these spectral changes resemble the ones observed upon deleting the CBD from TR (free TR $\Delta$ N; Figure S7D). Hence, they may, at least partially, reflect the modifications of interactions involving the remaining elements of TR upon sequestration of the CBD by CaM<sub>C</sub>. The potential implications of these interactions are discussed in detail in the section below.

## 3 | DISCUSSION

Kinetic, biochemical, and cell biological studies identified two specific events (illustrated in Figure S1A) that enable the activation of eEF-2K (and TR as its proxy).<sup>20</sup> The first of these events involves a conformational change driven by the engagement of Ca<sup>2+</sup>-CaM, greatly enhancing the ability to autophosphorylate on Thr348. The second post-chemistry event results from the engagement by pThr348 of an allosteric site (the PBP) on the KD that stabilizes a



**FIGURE 5** Time-course for the autophosphorylation of TR on Thr348 at pH 6.8 in the presence of  $\text{Ca}^{2+}$  (150  $\mu\text{M}$ ) and ATP (2 mM). Assays were performed at least twice and plotted as the fractional amount of Thr348 phosphorylation against time. (a) Western blot for TR autophosphorylation in the absence of CaM is shown on the top panel (pThr348 on top; total TR at the bottom shown as loading control). The corresponding fit to Equation (5) is shown in the bottom panel. The solid line corresponds to the best fit with  $k_{\text{auto}} = 0.0118 \pm 0.0009 \text{ min}^{-1}$  corresponding to a half-life of  $\sim 58.7 \text{ min}$ . (b) Western blot for the autophosphorylation of TR in the presence of saturating  $\text{CaM}_{\text{H107K}}$  (4  $\mu\text{M}$ ) is shown on the top panel (pThr348 on top; total TR at the bottom). The corresponding fit to Equation (5) is shown in the bottom panel. The solid line represents the best fit with  $k_{\text{auto}} = 0.29 \pm 0.037 \text{ min}^{-1}$  corresponding to a half-life of  $\sim 2.4 \text{ min}$ . (c) Western blot for the autophosphorylation of TR in the presence of saturating wild-type CaM (4  $\mu\text{M}$ ) is shown on the top panel (pThr348 on top; total TR at the bottom). The bottom panel shows that phosphorylation is rapid and complete within 0.17 min ( $\sim 10 \text{ s}$ )



conformation with the highest activity towards the substrate.<sup>20</sup> The precise mechanistic details of this two-step process are still mostly obscure. We have previously established the structural basis of the primary means through which eEF-2K recognizes CaM involving an interaction between the  $\text{Ca}^{2+}$ -free  $\text{CaM}_{\text{C}}$  and the so-called CBD on the N-terminus of the former.<sup>29</sup> When the CBD is a part of TR, rather than an isolated peptide, the primary interaction appears to be reinforced by a secondary one resulting in a significant enhancement in affinity that is further enhanced by the presence of  $\text{Ca}^{2+}$ <sup>30</sup>. Our current HXMS data suggest that this secondary interaction site is located on the  $\text{CaM}_{\text{C}}$  face opposite the one that recognizes the CBD.

We had previously utilized XLMS studies<sup>28</sup> to identify several intermolecular cross-links between  $\text{CaM}_{\text{N}}$  and  $\text{KD}_{\text{N}}$ , of which the best-defined one involved a linkage between K30 (protected in our present HXMS studies) on  $\text{CaM}_{\text{N}}$  and Glu145 on TR. Given the expected intimate interaction between  $\text{CaM}_{\text{C}}$  and TR, one could reasonably

expect that numerous intermolecular cross-links would also be identified between  $\text{CaM}_{\text{C}}$  and TR. Surprisingly, the only intermolecular  $\text{CaM}_{\text{C}}$  cross-link that could be confirmed involved E87 (that cross-links to Lys715 on the TR CTD). This residue is located in helix H on  $\text{CaM}_{\text{C}}$  in a region that shows increased protection from exchange upon TR binding at both pH\* values (Figure S2). Our current HXMS results suggest a high degree of protection for the hydrophobic part of  $\text{CaM}_{\text{C}}$  that recognizes the CBD and an additional surface that lies opposite it that is mostly hydrophilic and involves, in large part, all the four constituent helices. Therefore, it appears likely that  $\text{CaM}_{\text{C}}$  is almost entirely enveloped by TR with little solvent exposure when it is part of the UC, possibly explaining the lack of cross-links in the XLMS analysis. It is also notable that this secondary interaction site on  $\text{CaM}_{\text{C}}$  was not directly probed by our previous NMR studies of the interaction of CaM with TR given our reliance on Ile- $\delta$ 1 and Met- $\epsilon$  probes that exclusively line the hydrophobic face that engages the CBD.<sup>28,30</sup> However, it

is interesting that H107, deemed necessary for eEF-2K activation, is located on this surface and in the highly protected helix F therein.<sup>22</sup> That an H107K mutant of CaM is unable to effectively drive the conformational changes on TR required to enable efficient autophosphorylation on Thr348 could lead one to speculate that this secondary interaction is perhaps what is crucial in activating the kinase with the interaction involving the CBD merely serving as a tether to increase the local concentration of CaM near TR. The homologous  $\alpha$ -kinase domain from TRPM7 forms a head-to-head dimer utilizing an N-terminal helical extension.<sup>31</sup> Mutations within this extension variously affect dimerization and kinase activity.<sup>32</sup> Perhaps TR, and by inference, full-length eEF-2K, utilizes a similar mechanism with the CBD acting as the tether and CaM substituting for the second TRPM7 kinase domain.

Upon phosphorylation on Thr348 and transition from the UC to the PC, changes in protection on TR are modest, with the most significant being localized on KD<sub>C</sub>, an observation also supported by the corresponding NMR spectra. These complimentary studies suggest that autophosphorylation induces some local fine-tuning and overall stabilization of the TR catalytic machinery. For CaM, the most significant change in protection, an increase, is seen for CaM<sub>C</sub> and helix F therein, suggesting a modification of its interaction with TR involving the secondary surface upon Thr348 phosphorylation. Therefore, this observation likely highlights the tight integration of CaM<sub>C</sub> into the overall allosteric signaling pathway as part of the PC. Indeed, this is also the segment of CaM that is shown to respond to pH effects that have been deemed important in regulating the activity of eEF-2K.<sup>22</sup> Thus, based on the data in hand from our current and past analyses, it appears that CaM<sub>C</sub> not only forms the central platform for the assembly of the signaling complex involving TR, and by inference, eEF-2K, but it also acts as the primary long-range sensor of the allosteric network in responding to a variety of stimuli including phosphorylation and changes in pH.

Given the absence of experimentally determined three-dimensional structures of an intact TR or full-length eEF-2K, free or in complex with CaM, it is difficult to define the mechanism of the CaM-driven activation of TR (or eEF-2K) in atomic detail. However, based on our present and earlier results, we can speculate on the overall features of the activation process (shown schematically in Figure 6). One may conceive the interaction between CaM and TR to involve two distinct stages: (a) The recognition of the CBD by CaM<sub>C</sub> provides a majority of the binding free energy for the CaM/TR (or CaM/eEF-2K) interaction. The critical features of this interaction are captured by the structure of the

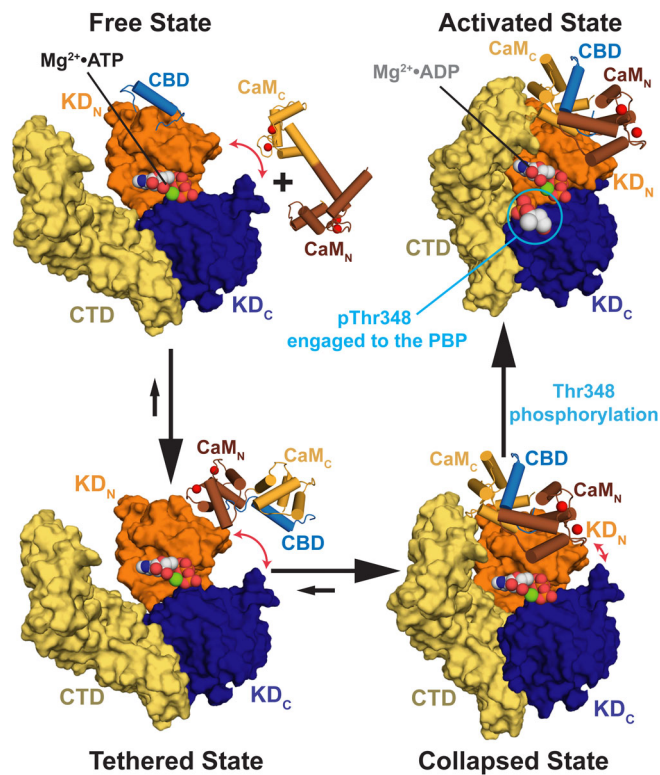


**FIGURE 6** Proposed model for the Ca<sup>2+</sup>-CaM-mediated activation of TR is shown schematically. Under high Ca<sup>2+</sup> conditions, Ca<sup>2+</sup>-loaded CaM (N-lobe, CaM<sub>N</sub>, brown; C-lobe, CaM<sub>C</sub>, light orange) engages the calmodulin-binding domain (CBD, blue) of TR through CaM<sub>C</sub>. This interaction tethers CaM to TR and results in the loss of the Ca<sup>2+</sup> ions bound to CaM<sub>C</sub>. This initial tethering is followed by the formation of a “collapsed” complex involving both the kinase domain (KD; N-lobe, KD<sub>N</sub>, dark orange; C-lobe, KD<sub>C</sub>, dark blue) and the C-terminal domain (CTD, yellow) of TR together with both lobes of CaM. CaM<sub>C</sub> plays a more dominant role in this collapse than CaM<sub>N</sub>. Formation of the collapsed complex also modifies intra-TR interactions between the KD and the CTD. The relative orientation between the two lobes of the KD (KD<sub>N</sub> and KD<sub>C</sub>) is also likely altered (red arrows), thus modifying their interface and the catalytic elements, including the ATP•Mg<sup>2+</sup> binding pocket, therein. The conformation of TR within this complex allows efficient autophosphorylation on Thr348. The subsequent engagement of the phosphate-binding pocket (PBP) by pThr348 leads to additional conformational changes, including further remodeling of the KD<sub>N</sub>/KD<sub>C</sub> interface, yielding a conformation with high activity towards the substrate. In this model, three distinct structural modules, CaM<sub>C</sub>, together with the KD and the CTD of TR, act as a single, connected allosteric unit

Ca<sup>2+</sup>-CaM•eEF-2K<sub>CBD</sub> complex.<sup>29</sup> This association provides a means to mutually tether CaM and TR, thus enhancing their local concentrations. (b) CaM and TR, now associated through the CBD tether, form a “collapsed” state in which CaM<sub>C</sub> engages TR through its secondary surface (as described above) and it is this interaction that drives the conformational transitions

necessary to allow the kinase to autophosphorylate on Thr348. While CaM<sub>N</sub> may also contribute to this collapse, as evident from its increased overall protection in the context of the UC, its role is likely to be primarily that of a Ca<sup>2+</sup>-sensor in modulating the overall affinity of the interaction; this latter role is likely to become more important under conditions of elevated pH especially in full-length eEF-2K (compared to TR, unpublished data). Within the collapsed complex, both in the context of the UC and the PC (though the precise structural details may be different for the two cases), the three primary contributing units, namely CaM<sub>C</sub>, the KD and the CTD of TR, appear to be structurally coupled. This is evident from the fact that phosphorylation on Thr348 and its subsequent engagement to the PBP triggers increased protection in CaM<sub>C</sub> (more specifically on helix F) and in the CTD (see Figures S3 and S5). While the structural details of the conformational changes induced on the TR KD upon CaM-binding and Thr348 phosphorylation are still unclear, based on our current and past<sup>28</sup> HXMS results, it is fair to assume that these processes involve changes in the relative orientations between KD<sub>N</sub> and KD<sub>C</sub> together with a remodeling of the ATP binding pocket. This hypothesis is supported by the increased protection seen in the loop connecting the two lobes both upon formation of the UC (see Figure 4 in reference<sup>28</sup> and then the PC (see Figure 2). The NMR spectral changes seen on the hinge (Ile232, see Figure 3) upon formation of the PC and at the interface between the two lobes (Ile214 and Ile237) provide further credence to this speculation. Additional lines of evidence are provided by biochemical studies suggesting that the apparent  $K_m$  towards Mg<sup>2+</sup>-ATP for free Thr348-phosphorylated eEF-2K is almost an order of magnitude lower than that when complexed with Ca<sup>2+</sup>-CaM.<sup>20</sup> Changes in the inter-lobe orientation and remodeling of their interface have been suggested to be critical in the activation of many kinases.<sup>33,34</sup> Indeed, such a mechanism involving the closure of the nucleotide-binding pocket has been associated with the activation of the eEF-2K homolog, myosin heavy chain kinase A (MHCK-A).<sup>35,36</sup> Confirmation or further refinement of this model awaits high-resolution structural information on free TR (or eEF-2K) and the corresponding UCs and PCs.

## 4 | MATERIALS AND METHODS

### 4.1 | Preparation of the inactive and active complexes

CaM and unphosphorylated TR were prepared as described previously.<sup>28</sup> To prepare the unphosphorylated

complex (UC), TR was incubated at pH 7.5 with a three-fold excess of CaM in the presence of a large excess (10 mM) of CaCl<sub>2</sub>. The 1:1 Ca<sup>2+</sup>-CaM•TR complex representing the UC was then isolated by injecting the mixture into a gel-filtration column (Superdex 75, prep grade, GE Healthcare Biosciences) equilibrated with 20 mM Tris, pH 7.5, 200 mM NaCl, 2 mM DTT, 1.0 mM CaCl<sub>2</sub> (HXMS buffer). To phosphorylate TR on Thr348, ~100 μM of TR was incubated with ~300 μM CaM for 30 min at room temperature in the presence of 40 mM MgCl<sub>2</sub> and 20 mM ATP. The reaction was quenched by 20-fold dilution into the corresponding Ca<sup>2+</sup>-free buffer and adding an excess (20 mM) of EDTA. Excess nucleotides were then removed through five buffer exchange steps in the presence of EDTA using spin columns with a 3.0 kDa cutoff. This was followed by an excess of CaCl<sub>2</sub> (20 mM) and the resulting complex was then isolated by gel filtration. ESI-MS performed on the intact protein and the pepsin-digested peptides confirmed the complete phosphorylation on Thr348 and the lack of phosphorylation at additional sites.

### 4.2 | Hydrogen/deuterium exchange mass spectrometry (HXMS) measurements

HXMS experiments utilized starting solutions consisting of ~100 μM each of UC, PC, or free Ca<sup>2+</sup>-CaM in the HXMS buffer. These samples were diluted 25-fold at 15°C into D<sub>2</sub>O-based buffer either at pH\* (the “\*” indicates that the pH value was obtained through direct measurement) 6.2 or 7.6.<sup>37</sup> 20 mM MES and 20 mM Tris were used for the buffers at the low and high pH values, respectively, that were otherwise identical in composition to the H<sub>2</sub>O-based HXMS buffer. Incubation times were set to 1, 15, 30, and 60 min; all timepoints were collected either in duplicate or triplicate. Complete datasets for each of the three samples (UC, PC, or free Ca<sup>2+</sup>-CaM) were collected for a given timepoint before proceeding to the next time point. All sample handling was performed using a LEAP HDX PAL robotic system (Trajan Scientific) but otherwise following previously described protocols.<sup>28</sup> The exchange was quenched by diluting the samples with an equal volume solution of 0.4% formic acid in H<sub>2</sub>O. The mixture was then injected into a loop through an Enzymate BEH Pepsin column (Waters) using an aqueous loading buffer containing 2% acetonitrile and 0.2% formic acid and a flow rate of 0.1 mL/min for 2 min. The pepsin column was mounted inline of a 10 μL C8Opti-lynx II trap cartridge (Optimize Technologies). The peptides thus generated were first washed with the same loading buffer using a flow rate of 0.15 mL/min for 1 min and eluted using a flow rate of 0.04 mL/min

employing the following protocol: 11 min of a 0% to A:B 50% gradient (A: water/acetonitrile/formic acid, 97%/3%/0.15%; B: water/acetonitrile/formic acid, 3%/97%/0.15%) followed by 2 min of 50% to 100% of the same A:B gradient onto an inline 50 × 1-mm Hypersil Gold C18 column (Thermo Scientific) leading directly into a maXis-II ETD ESI-QqTOF spectrometer. For each sample, MS/MS data were obtained from a reference run where the proteins were diluted into aqueous buffers, and no  $^2\text{H}$  exchange was performed. The peptide fragments were identified using Bruker COMPASS and BIO-TOOLS software packages. The degree of  $^2\text{H}$  incorporation and charge states for the various peptides were assessed using the commercial software HDExaminer 2.4 (Sierra Analytics), as described previously.<sup>28</sup> The difference heatmaps for  $^2\text{H}$  levels between distinct states were calculated only when the values were statistically significant; the percentage  $^2\text{H}$  incorporation was calculated with respect to a specific reference state (e.g., free  $\text{Ca}^{2+}$ -CaM or the UC). A “moderate” smoothing function was applied to all difference maps.

### 4.3 | NMR spectroscopy

TR, specifically  $^{13}\text{C}, ^1\text{H}$ -labeled at the Ile- $\delta 1$  position in an otherwise uniformly  $^2\text{H}$ -labeled background (I-labeled), uniformly  $^2\text{H}$ -labeled or IM-labeled ( $^{13}\text{C}, ^1\text{H}$ -labeled at the Ile- $\delta 1$  position and  $^{13}\text{C}$ -labeled at the Met- $\epsilon$  position, all other positions are  $^2\text{H}$ ) CaM were expressed and purified as described elsewhere.<sup>30</sup>  $^2\text{H}$ -labeled or IM-labeled  $\text{CaM}_{\text{H107K}}$  were expressed and purified in a fashion similar to wild-type CaM.  $^{13}\text{C}, ^1\text{H}$  HMQC spectra of I-labeled TR alone or in the presence of 3 molar equivalents of  $^2\text{H}$ -labeled  $\text{CaM}_{\text{H107K}}$  were acquired at 700 MHz in a buffer containing 20 mM BisTris pH 6.8, 150 mM KCl, 10 mM  $\text{CaCl}_2$ , 5 mM  $\beta$ -mercaptoethanol and 0.1%  $\text{NaN}_3$  (NMR buffer prepared in 100%  $\text{D}_2\text{O}$ ). Corresponding spectra of a 1:1 complex of I-labeled TR and  $^2\text{H}$ -labeled wild-type CaM were acquired at 800 MHz.

Phosphorylation of TR on Thr348 was achieved by adding 10 mM  $\text{MgCl}_2$  and 1 mM ATP to a 1:1 complex comprising I-labeled TR and  $^2\text{H}$ -labeled CaM. After 5 min incubation, the complex was diluted into  $\text{Ca}^{2+}$ -free NMR buffer. The sample was exchanged twice into the same buffer, followed by three exchanges into the NMR buffer using spin columns with a 3.0 kDa cutoff. Spectra of I-labeled TR or pTR, in the apo form, or bound to  $^2\text{H}$ -labeled CaM, representing the UC and the PC, respectively, were acquired at 700 MHz. All NMR spectra were collected at 25°C on Bruker Avance III spectrometers equipped with cryogenic probes capable of applying

pulsed-field gradients along the z-axis, processed using nmrPipe<sup>38</sup> and analyzed using nmrViewJ.<sup>39</sup>

### 4.4 | Measurement of autophosphorylation

Auto-phosphorylation of TR was carried out in the absence or the presence of either wild-type CaM or  $\text{CaM}_{\text{H107K}}$  (4  $\mu\text{M}$ ) at pH 6.8 in assay buffer [HEPES (25 mM), KCl (50 mM),  $\text{MgCl}_2$  (11 mM),  $\text{CaCl}_2$  (1.15 mM), EGTA (1 mM), BSA (20  $\mu\text{g}/\text{mL}$ ), and DTT (2 mM)] containing TR (222 nM). The concentrations of free  $\text{Ca}^{2+}$  and  $\text{Mg}^{2+}$  were approximately 150  $\mu\text{M}$  and 10 mM, respectively (calculated using the Maxchelator program<sup>40</sup>). Reaction mixtures were incubated for 10 min at 30°C before initiating the reaction by adding ATP (2 mM). Aliquots were removed at specified time intervals and quenched in hot SDS-PAGE sample loading buffer, glycerol (4%, vol/vol),  $\beta$ -mercaptoethanol (2%, vol/vol), SDS (0.8%), bromophenol blue (0.004%), and Tris-Cl (pH 6.75, 25 mM). Samples (100 ng TR) were analyzed by immunoblotting. PVDF membranes were labeled overnight with anti-eEF-2K total mouse (Santa Cruz; to quantify total TR) and anti-phosphoThr348-eEF-2K rabbit (ECM biosciences; to quantify TR phosphorylated on Thr348) antibodies diluted in TBS tween (TBST) containing 5% BSA. After primary antibody labeling, the membranes were incubated with secondary anti-mouse and anti-rabbit antibodies (Li-COR) prepared in TBST. The membranes were imaged using an Odyssey Li-COR imager and analyzed with Image Studio software. The intensity at a given time point was normalized to the maximum measured signal, and the reaction progress was plotted against time. The data were fitted to Equation (5) to determine the approximate rate of Thr348 autophosphorylation.

$$F(t) = F_{\infty} (1 - e^{-k_{\text{auto}} t}) \quad (5)$$

where  $F(t)$  is the fraction phosphorylated at a given time  $t$  and  $F_{\infty}$  is the limiting fractional phosphorylation. The corresponding half-life is  $t_{1/2} = \ln(2)/k_{\text{auto}}$ .

### ACKNOWLEDGMENTS

This work is supported by NIH awards R01 GM123252 (to RG and KND) and the Welch Foundation F-1390 (KND). KL was partially supported by a pre-doctoral fellowship (15PRE25760018) from the American Heart Association. All NMR and MS experiments were carried out at the ASRC NMR and MS facilities, respectively.

## AUTHOR CONTRIBUTIONS

**Andrea Piserchio:** Formal analysis; investigation; methodology; validation; visualization; writing-original draft. **Kimberly Long:** Methodology; validation. **Kwangwoon Lee:** Formal analysis; validation; writing-review & editing. **Eric Kumar:** Methodology. **Rinat Abzalimov:** Investigation; methodology. **Kevin Dalby:** Conceptualization; funding acquisition; resources; supervision; writing-review & editing. **Ranajeet Ghose:** Conceptualization; funding acquisition; resources; supervision; writing-review & editing.

## ORCID

Ranajeet Ghose  <https://orcid.org/0000-0002-0763-8686>

## REFERENCES

- Hershey JW. Translational control in mammalian cells. *Annu Rev Biochem.* 1991;60:717–755.
- Morley SJ, Thomas G. Intracellular messengers and the control of protein synthesis. *Pharmacol Ther.* 1991;50:291–319.
- Proud CG. Protein phosphorylation in translational control. *Curr Top Cell Regul.* 1992;32:243–369.
- Rhoads RE. Signal transduction pathways that regulate eukaryotic protein synthesis. *J Biol Chem.* 1999;274:30337–30340.
- Browne GJ, Proud CG. Regulation of peptide-chain elongation in mammalian cells. *Eur J Biochem.* 2002;269:5360–5368.
- Dever TE, Green R. The elongation, termination, and recycling phases of translation in eukaryotes. *CSH Perspect Biol.* 2012;4:a013706.
- Kaul G, Pattan G, Rafeequi T. Eukaryotic elongation factor-2 (eEF2): Its regulation and peptide chain elongation. *Cell Biochem Funct.* 2011;29:227–234.
- Tanaka M, Iwasaki K, Kaziro Y. Translocation reaction promoted by polypeptide chain elongation factor-2 from pig liver. *J Biochem.* 1977;82:1035–1043.
- Ryazanov AG, Pavur KS, Dorovkov MV. Alpha-kinases: A new class of protein kinases with a novel catalytic domain. *Curr Biol.* 1999;9:R43–R45.
- Ryazanov AG, Ward MD, Mendola CE, et al. Identification of a new class of protein kinases represented by eukaryotic elongation factor-2 kinase. *Proc Natl Acad Sci U S A.* 1997;94:4884–4889.
- Nairn AC, Bhagat B, Palfrey HC. Identification of calmodulin-dependent protein kinase III and its major Mr 100,000 substrate in mammalian tissues. *Proc Natl Acad Sci U S A.* 1985;82:7939–7943.
- Nairn AC, Palfrey HC. Identification of the major Mr 100,000 substrate for calmodulin-dependent protein kinase III in mammalian cells as elongation factor-2. *J Biol Chem.* 1987;262:17299–17303.
- Ryazanov AG. Ca<sup>2+</sup>/calmodulin-dependent phosphorylation of elongation factor 2. *FEBS Lett.* 1987;214:331–334.
- Ryazanov AG, Davydova EK. Mechanism of elongation factor 2 (EF-2) inactivation upon phosphorylation. Phosphorylated EF-2 is unable to catalyze translocation. *FEBS Lett.* 1989;251:187–190.
- Ryazanov AG, Shestakova EA, Natapov PG. Phosphorylation of elongation factor 2 by EF-2 kinase affects rate of translation. *Nature.* 1988;334:170–173.
- Ryazanov AG, Natapov PG, Shestakova EA, Severin FF, Spirin AS. Phosphorylation of the elongation factor 2: The fifth Ca<sup>2+</sup>/calmodulin-dependent system of protein phosphorylation. *Biochimie.* 1988;70:619–626.
- Carlberg U, Nilsson A, Nygard O. Functional properties of phosphorylated elongation factor 2. *Eur J Biochem.* 1990;191:639–645.
- Dumont-Miscopein A, Lavergne JP, Guillot D, Sontag B, Reboud JP. Interaction of phosphorylated elongation factor EF-2 with nucleotides and ribosomes. *FEBS Lett.* 1994;356:283–286.
- Stratton MM, Chao LH, Schulman H, Kuriyan J. Structural studies on the regulation of Ca<sup>2+</sup>/calmodulin dependent protein kinase II. *Curr Opin Struct Biol.* 2013;23:292–301.
- Tavares CDJ, Ferguson SB, Giles DH, et al. The molecular mechanism of eukaryotic elongation factor 2 kinase activation. *J Biol Chem.* 2014;289:23901–23916.
- Tavares CD, Giles DH, Stancu G, et al. Signal integration at elongation factor 2 kinase; the roles of calcium, calmodulin and Ser-500 phosphorylation. *J Biol Chem.* 2017;292:2032–2045.
- Xie J, Mikolajek H, Pigott CR, et al. Molecular mechanism for the control of eukaryotic elongation factor 2 kinase by pH: Role in cancer cell survival. *Mol Cell Biol.* 2015;35:1805–1824.
- Redpath NT, Price NT, Severinov KV, et al. Regulation of elongation factor-2 by multisite phosphorylation. *Eur J Biochem.* 1993;213:689–699.
- Leprivier G, Remke M, Rotblat B, et al. The eEF2 kinase confers resistance to nutrient deprivation by blocking translation elongation. *Cell.* 2013;153:1064–1079.
- Meric-Bernstam F, Chen H, Akcakanat A, et al. Aberrations in translational regulation are associated with poor prognosis in hormone receptor-positive breast cancer. *Breast Cancer Res.* 2012;14:R138.
- Kavalali ET, Monteggia LM. Synaptic mechanisms underlying rapid antidepressant action of ketamine. *Am J Psychiatry.* 2012;169:1150–1156.
- Monteggia LM, Gideons E, Kavalali ET. The role of eukaryotic elongation factor 2 kinase in rapid antidepressant action of ketamine. *Biol Psychiatry.* 2013;73:1199–1203.
- Will N, Lee K, Hajredini F, et al. Structural dynamics of the activation of elongation factor 2 kinase by Ca<sup>2+</sup>-calmodulin. *J Mol Biol.* 2018;430:2802–2821.
- Lee KH, Alphonse S, Piserchio A, et al. Structural basis for the recognition of eukaryotic elongation factor 2 kinase by calmodulin. *Structure.* 2016;24:1441–1451.
- Lee K, Kumar EA, Dalby KN, Ghose R. The role of calcium in the interaction between calmodulin and a minimal functional construct of eukaryotic elongation factor 2 kinase. *Protein Sci.* 2019;28:2089–2098.
- Yamaguchi H, Matsushita M, Nairn AC, Kuriyan J. Crystal structure of the atypical protein kinase domain of a TRP channel with phosphotransferase activity. *Mol Cell.* 2001;7:1047–1057.
- Crawley SW, Cote GP. Identification of dimer interactions required for the catalytic activity of the TRPM7 alpha-kinase domain. *Biochem J.* 2009;420:115–122.

33. Johnson LN, Noble ME, Owen DJ. Active and inactive protein kinases: Structural basis for regulation. *Cell*. 1996;85:149–158.
34. Barr D, Oashi T, Burkhard K, et al. Importance of domain closure for the autoactivation of ERK2. *Biochemistry*. 2011;50:8038–8048.
35. Ye Q, Crawley SW, Yang Y, et al. Crystal structure of the alpha-kinase domain of Dictyostelium myosin heavy chain kinase A. *Sci Signal*. 2010;3:ra17.
36. Ye Q, Yang Y, van Staalduinen L, et al. Structure of the *Dictyostelium* myosin-II heavy chain kinase A (MHCK-A) alpha-kinase domain apoenzyme reveals a novel autoinhibited conformation. *Sci Rep*. 2016;6:26634.
37. Coales SJ, SY E, Lee JE, et al. Expansion of time window for mass spectrometric measurement of amide hydrogen/deuterium exchange reactions. *Rapid Commun Mass Spectrom*. 2010;24:3585–3592.
38. Delaglio F, Grzesiek S, Vuister GW, Zhu G, Pfeifer J, Bax A. NMRPipe: A multidimensional spectral processing system based on UNIX pipes. *J Biomol NMR*. 1995;6:277–293.
39. Johnson BA. From raw data to protein backbone chemical shifts using NMRfX processing and NMRViewJ analysis. *Meth Mol Biol*. 2018;1688:257–310.
40. Patton C, Thompson S, Epel D. Some precautions in using chelators to buffer metals in biological solutions. *Cell Calcium*. 2004;35:427–431.
41. Devkota AK, Edupuganti R, Yan C, et al. Reversible covalent inhibition of eEF-2K by carbonitriles. *ChemBioChem*. 2014;15:2435–2442.

## SUPPORTING INFORMATION

Additional supporting information may be found online in the Supporting Information section at the end of this article.

**How to cite this article:** Piserchio A, Long K, Lee K, Kumar EA, Abzalimov R, Dalby KN, Ghose R. Structural dynamics of the complex of calmodulin with a minimal functional construct of eukaryotic elongation factor 2 kinase and the role of Thr348 autophosphorylation. *Protein Science*. 2021;30:1221–1234. <https://doi.org/10.1002/pro.4087>